Pump-and-probe studies of the $E1(6\,^3S_1)\leftarrow A0^+(5\,^3P_1)$ excitation spectrum of CdAr in a supersonic beam

M. Czajkowski, R. Bobkowski, and L. Krause
Department of Physics, University of Windsor, Windsor, Ontario, Canada N9B 3P4
(Received 11 October 1991)

The pump-and-probe method of laser spectroscopy in conjunction with a jet-expansion molecular beam was used to record the excitation spectrum arising from $E1(6\,^3S_1)\leftarrow A0^+(5\,^3P_1)$ vibronic transitions in the CdAr excimer. Two lasers were employed for the two-step excitation. A Nd:YAG (where YAG denotes yttrium aluminum garnet) laser-pumped dye laser (pump laser) was tuned to the $A0^+(v=5)\leftarrow X0^+(v=0)$ transition, producing a population of the $A0^+$ state that was subsequently excited with a N_2 laser-pumped dye laser (probe laser) to the $E1(6\,^3S_1)$ state. The probe laser was scanned in the range 4735–5060 Å, producing a vibronic excitation spectrum that consisted of about 20 components. The spectrum was subjected to vibrational analysis, and the assignments of the components were made with the aid of a computer-simulated spectrum based on Franck-Condon factors calculated assuming the Morse potential as representative of the upper and lower states. The analysis yielded D_e, ω_e, $\omega_e x_e$, and r_e for the $E1$ state. The potential-energy curve for the $E1$ state is compared with a theoretical curve calculated by Czuchaj and Sienkiewicz [J. Phys. B **17**, 225 (1984)] and by Czuchaj, Stoll, and Preuss [J. Phys. B **20**, 1487 (1986)].

PACS number(s): 33.20.Lg

I. INTRODUCTION

In recent years there has been an increasing interest in the vibronic spectroscopy of van der Waals molecules composed of group II metal atoms and noble gases (X), as indicated by numerous reports in the literature [1–13]. For example, Hg-X complexes were studied in cold expansion beams [14,1–5], and Cd-X molecules were similarly investigated [6–9], as were the Zn-X [10], Zn_2 [11,12], and Cd_2 [13] species. Laser spectroscopy of van der Waals complexes provides a very useful means for the study of these very weakly bound species and permits the determination of various spectroscopic constants, including the equilibrium internuclear separation r_e and the dissociation energy. The vibronic and rovibronic spectra can also be used to produce molecular potential-energy (PE) curves. While one-step laser excitation generally permits the study of the low-lying molecular states, the pump-and-probe (two-step) excitation method can be used to produce laser-induced fluorescence (LIF) from more highly excited states that have r_e lengths comparable with that of the ground state [15], provided that the Franck-Condon (FC) factors are of sufficient magnitude for both the "pump" and "probe" excitation steps.

Laser spectroscopy of van der Waals molecules may also be used to interpret various dynamical phenomena such as collisional excitation transfer, quenching, and energy transfer in chemical reactions [15]. These species also provide an interesting and still largely unexplored field for theoretical studies, since there appear to be only two reports in the literature dealing with Cd-X systems [14], which provide a limited opportunity to check quantum-mechanical calculations against experimental results.

In this report we present spectroscopic data obtained by the pump-and-probe method which we used to populate the $E1(6\,^3S_1)$ state of CdAr. The experimental results are employed to construct PE curves that can be directly compared with those calculated by Czuchaj and co-workers [14].

II. EXPERIMENTAL DETAILS

A. Description of the apparatus

The arrangement of the apparatus used in the pump-and-probe experiments is shown in Fig. 1. The CdAr molecules produced in the expansion beam [13] were irradiated with two successive laser (pump and probe) pulses. The pump radiation was generated with an in-house-built dye laser excited with the third harmonic output (3350 Å) of a Quanta-Ray Nd:YAG (where YAG denotes yttrium aluminum garnet) laser. The dye-laser output (6534 Å) was frequency-doubled to produce the 3267-Å pump radiation which was tuned to produce the maximal population of $A0^+(5\,^3P_1)$, $v=5$ molecules by excitation from the $X0^+(5S_0)$ ground state [9]. The molecules were excited further to the $E1(6\,^3S_1)$ state by the probe pulses emitted from a second dye laser pumped with an (in-house-built) N_2 laser. The probe pulses were delayed by approximately 350 ns with respect to the pump pulses. The resulting LIF, emitted perpendicularly to the directions of the molecular beam and the laser beams, was detected with a Hamamatsu R2496 photomultiplier which was screened from the intense pump radiation by a uv absorbing filter. The photomultiplier signal was registered with an EG & G model No. 162/166 boxcar integrator and recorded with an X-Y plotter. The boxcar

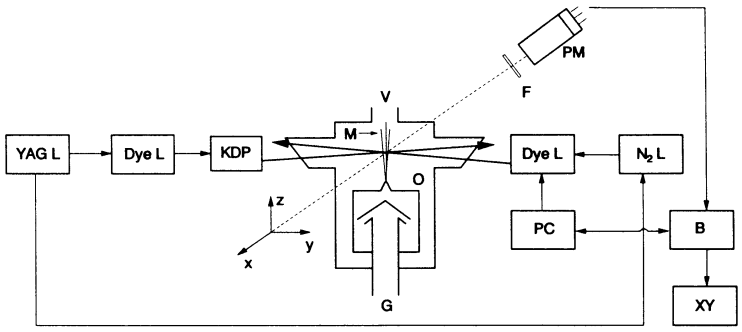

FIG. 1. Arrangement of the apparatus used in the pump-and-probe experiments: O, source oven; M, molecular beam; PC, microcomputer; B, boxcar integrator (or transient digitizer); F, uv filter; PM, photomultiplier; G, Ar supply; V, vacuum line.

window had a 50-ns width and partly overlapped the probe pulses, to make possible the detection of the LIF emitted from the $E1$ state which has a lifetime of a few nanoseconds while the $A0^+$ state has a lifetime of about 2.5 μs. In experiments in which we measured the lifetime of the $E1$ state, the boxcar integrator was replaced with a Hewlett-Packard model No. 5411D digitizing oscilloscope used as a transient digitizer. The experiment was controlled by an in-line-connected PC XT computer which scanned the probe dye laser over predetermined wavelength limits and stored the output of the boxcar integrator or transient digitizer.

B. Properties of the supersonic beam

Both the pump and the probe laser beams, directed roughly antiparallel to each other, were focused at the center of the molecular beam, at a well-defined distance (X) measured from the oven nozzle [16]. Figure 2 shows schematically a Campargue barrel-shaped beam produced at a chamber pressure of about 90 mTorr measured with the beam "on" and about 1 mTorr with the beam "off." The source (oven) was maintained at a temperature $T_0=950$ K which corresponded to a Cd vapor pressure of about 250 Torr, and the backing pressure P_0 of Ar, the carrier gas, was 11.25 atm. During the expansion through the orifice (whose diameter was $D=1.8\times10^{-2}$ cm), the temperature as well as the densities of Ar and Cd atoms decreased with increasing distance X from the nozzle, as did the collision rate in the beam. This rate eventually reached a limit beyond which no further cooling took place and at which the axial velocity distribution and the Mach number (the ratio of the beam velocity to the local speed of sound which is proportional to the square root of the temperature) reached their terminal values.

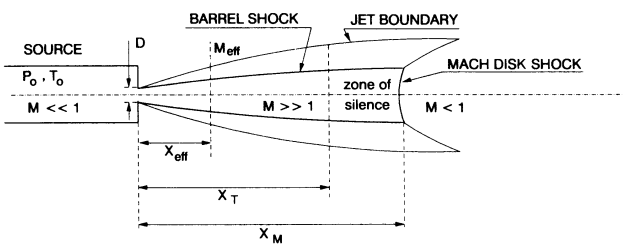

FIG. 2. Schematic cross section of a jet-expansion beam. M designates the appropriate Mach number.

The terminal Mach number M_T may be obtained from the expression [17]

$$M_T=133(P_0D)^{0.4}\ , \tag{1}$$

where P_0 is stated in atm and D in cm. The distance X_T corresponding to M_T is given by

$$M_T=3.26\left[\frac{X_T}{D}\right]^{0.67}\ . \tag{2}$$

The conditions prevailing in our experiment resulted in the values $M_T=70$ and $X_T=1.8$ cm. The effective Mach number $M_{\rm eff}$ at a point in the beam between the nozzle and X_T depends on X and is given by

$$M_{\rm eff}\cong3.26\left[\frac{X}{D}\right]^{0.67}\ . \tag{3}$$

The excitation spectrum was recorded using the following sets of beam parameters which crucially affected the spectral intensity profile:

(a) $X=0.6$cm, $X/D=33$, $M_{\rm eff}=34$;

(b) $X=0.8$cm, $X/D=44$, $M_{\rm eff}=41$;

(c) $X=1.13$cm, $X/D=62$, $M_{\rm eff}=52$.

The density of Ar atoms at the point of excitation is given by

$$n=n_0[1+\tfrac{1}{2}(\gamma-1)M_{\rm eff}^2]^{-1/(\gamma-1)}\ , \tag{4}$$

where $\gamma=1.67$ and $n_0=8.75\times10^{19}$ is the Ar density at P_0 and T_0. At $X=0.6$cm, $n=1.12\times10^{16}$cm^{-3}. Z, the collision frequency per CdAr molecule under the same conditions in the expansion beam, may be obtained from using the relation

$$Z=\sqrt{2}n\sigma\bar{v}\ , \tag{5}$$

where

$$\bar{v}=\bar{v}_0[1+\tfrac{1}{2}(\gamma-1)M_{\rm eff}^2]^{-1/2} \tag{6}$$

and $\bar{v}_0$ is the average speed of Ar atoms at 950 K, yielding $\bar{v}=4.2\times10^3$ cm/s. The "hard-sphere" collision cross section σ was estimated from the sum of the average diameters $d_{Ar}=3.5$ Å and $d_{CdAr}=7.0$Å [8], which yields the average collision radius $R=5$ Å,

$$\sigma=\pi R^2=80\times10^{-16}\text{cm}^2 ,$$

and $Z=5.3\times10^5\ \text{s}^{-1}$ collisions per $A0^+(5\,^3P_1)$ molecule. Since the lifetime τ of the $A0^+$, $v=5$ state is 2.7×10^{-6} s [8], this translates into about 1.5 collisions per lifetime, indicating that the $A0^+$ molecule suffers at least one collision before decaying to the ground state. Similar considerations suggest that, for $M_{\text{eff}}=52$, there are 0.2 collisions per lifetime and, on the other hand, if $X<0.6$ cm, the collision frequency will increase, populating additional vibrational states and giving rise to a more complex fluorescence spectrum. As will be seen below, these predictions are well verified by experimental results. As X increased, the density of the CdAr molecules decreased rapidly and so did the fluorescence signal. It would have been desirable to excite the fluorescence at $X\geq X_T$ but, even at $X=1.15$ cm, the intensity of the LIF became too faint to be detected.

III. RESULTS AND DISCUSSION

A. Description of the excitation spectrum

Figure 3 shows the energy levels involved in the pump-and-probe process, as well as the relevant transitions. The pump radiation excited the $A0^+(5\,^3P_1)$, $v=5$ vibronic state of CdAr, and collisions of these excited molecules, taking place in the expansion beam, populated some of the neighboring vibrational levels. The choice of the $v=5$ state for pump excitation was motivated by the large FC factor for the

$$A0^+(v=5)\leftarrow X0^+(v=0)$$

transition [8]. The probe radiation excited the vibronic $E1(6\,^3S_1)$ states which decayed to the $A0^+$, $B1(^3P_1)$, and $C2(^3P_2)$ states emitting detectable fluorescence. The $A0^+\rightarrow X0^+$ decay gave rise to fluorescence emission in the ultraviolet region, resulting from the bound-free transition which terminated on the repulsive part of the $X0^+$ PE curve. This uv continuum fluorescence, which was observed in the region extending over 200 Å from the Cd($5\,^3P_1\rightarrow5\,^1S_0$) resonance line towards longer wavelengths, was prevented from reaching the photomultiplier (PM) tube by a uv-absorbing filter. As the probe laser was scanned through the excitation region, the fluorescence emission was monitored producing an excitation spectrum whose traces, corresponding to the various expansion-beam parameters, are shown in Fig. 4. The trace in Fig. 4 (a) shows a spectrum that was obtained with $X/D=33$ and that was very much influenced by collisions of the $A0^+$, $v''=5$ molecules with Ar atoms, which populated the $v''=2$, 3, and 4 vibrational levels and gave rise to broad vibrational components shaded (degraded) towards shorter wavelengths. The profiles of the vibrational components suggest also a high rotational temperature in the expansion beam. To simplify the excitation spectrum, we carried out additional recordings with $X/D=44$, 62, and 72. The traces corresponding to $X/D=44$ and 62 are shown in Figs. 4(b) and 4(c), respectively, but we were not able to record any useful signal at $X/D=72$. The trace in Fig. 4(b) represents an intermediate case, where the vibrational components due to the collisionally excited v'' levels are at the point of vanishing; the trace in Fig. 4(c) does not include any such components and provided the basis for the vibrational analysis. The varying intensities of the spectrum presented in the three traces are due to the fact that each trace was recorded in a separate experiment and the source oven was cleaned, refilled, and realigned between the individual runs.

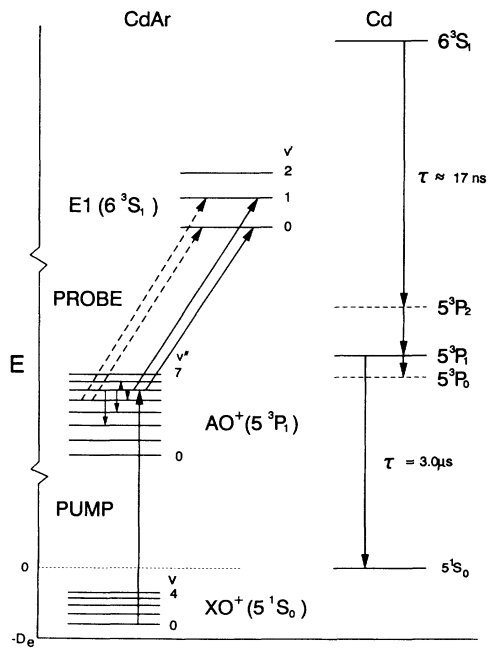

FIG. 3. A partial schematic CdAr and Cd energy-level diagram showing pump-and-probe excitation, $A0^+$ vibrational relaxation, and atomic decays.

B. Determination of the molecular constants for the $E1$ state

The vibrational analysis of the spectrum shown in Fig. 4(c) was based on the reasonable assumption that the spectrum represented an $E1$, $v'\leftarrow A0^+$, $v''=5$ vibrational progression with the component at 5057 Å corresponding to the $v'=0\leftarrow v''=5$ transition. The wave numbers, assignments, and separations of the vibronic components of the spectrum are listed in Table I and the Birge-Sponer plot of $\Delta G(v'+\frac{1}{2})$ against v' is shown in Fig. 5(a). Extrapolation of ΔG to $v'=0$ and $v'=v'_D$ (the highest vibrational level before the dissociation limit) yields ω'_0, $\omega'_0x'_0$, and v'_D, with the anharmonicity $\omega'_0x'_0$ given by the slope. The resulting dissociation energy D'_0 for the $E1$ state was 1248 cm^{-1}. However, as may be seen in Fig. 5(a), the Birge-Sponer plot is not strictly linear and exhibits a slight curvature near the dissociation limit. The dissocia-

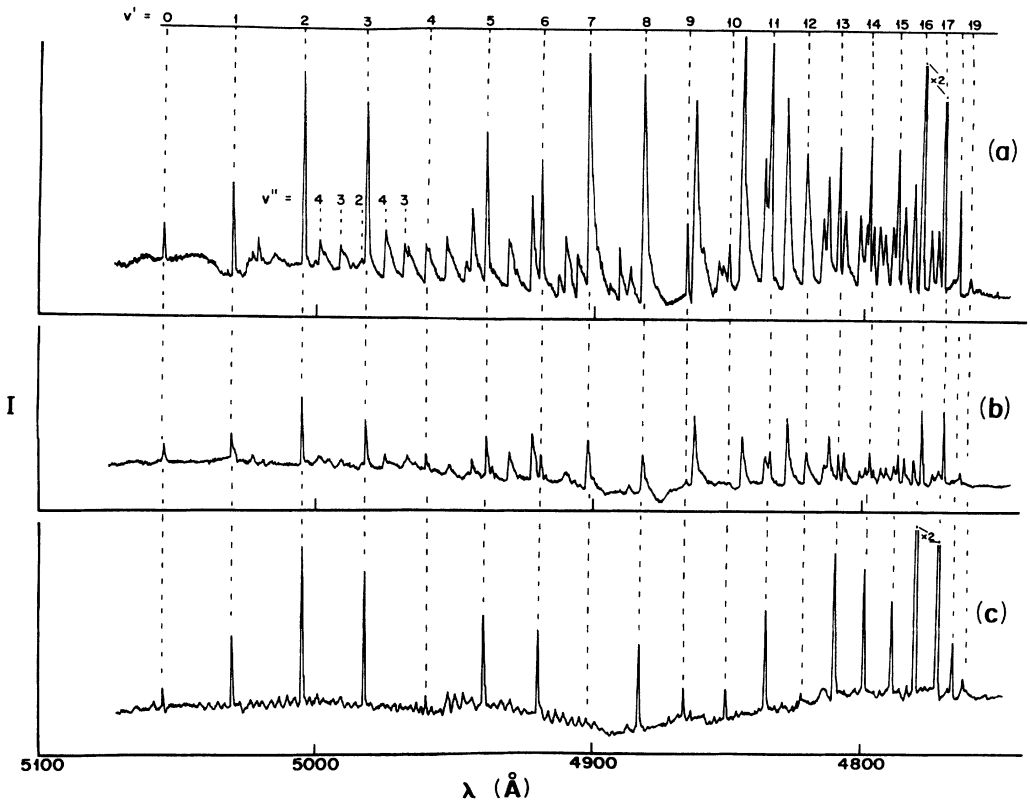

FIG. 4. The $E1(6\,^3S_1)$, $v' \leftarrow A0^+(5\,^3P_1)$, $v''=5$ excitation spectrum of CdAr. (a) $X/D=33$; (b) $X/D=44$; (c) $X/D=62$. The trace (a) includes v'' progressions due to collisionally populated v'' levels. The amplification factor of the boxcar has been doubled for $\lambda > 4820$ Å.

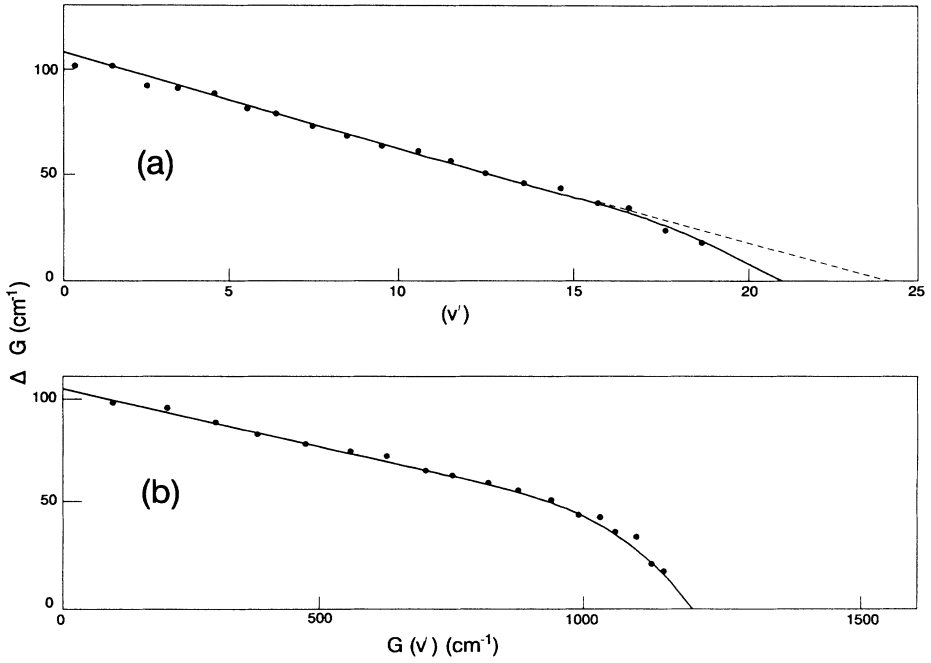

FIG. 5. (a) A Birge-Sponer plot of the v' progression in the $E1 \leftarrow A0^+$ excitation spectrum; (b) a plot of $\Delta G(v')$ against $G(v')$.

TABLE I. Frequencies of $E1$, $v' \leftarrow A0^+$, $v''=5$ vibronic bands.

v'	$\tilde{\nu}$ (cm^{-1})	$\Delta G(v')$ (cm^{-1})
0	19 780.1	99.4
1	19 879.5	102.0
2	19 982.0	90.7
3	20 072.6	91.0
4	20 163.6	88.0
5	20 251.6	81.3
6	20 332.9	79.6
7	20 412.5	75.9
8	20 488.4	66.5
9	20 554.9	65.5
10	20 620.3	62.7
11	20 683.0	55.2
12	20 738.2	52.6
13	20 790.8	48.0
14	20 838.8	45.8
15	20 884.6	36.6
16	20 921.2	36.3
17	20 957.5	23.7
18	20 981.2	20.0
19	21 001.2	

tion energy corrected for this curvature was obtained from the relation

$$D_0'(\text{corrected}) = \frac{A_2}{A_1}(1248\ \text{cm}^{-1}) = 1197\ \text{cm}^{-1}\ , \tag{7}$$

where A_2 is the measured area under the curved plot and A_1 is the area under the extrapolated linear plot.

As an alternative to plotting $\Delta G(v'+\frac{1}{2})$ against v', it is sometimes useful to plot $\Delta G(v'+\frac{1}{2})$ against the total vibrational energy $G(v)$ [18], obtaining a roughly parabolic curve which can be extrapolated to produce an intercept on the $G(v')$ axis, yielding directly the dissociation energy. Such a plot, which is shown in Fig. 5(b), yielded $D_0' = 1200\ \text{cm}^{-1}$, in good agreement with the corrected value derived from the Birge-Sponer plot.

The dissociation energy for the $E1$ state can also be obtained from the relation

$$D_0'(E1) = \mathcal{E}(6\,^3S_1) + D_0(A0^+) - \mathcal{E}(5\,^3P_1) - \tilde{\nu}_{00}(E1 \leftarrow A0^+)\ , \tag{8}$$

where $D_0(A0^+) = 303\ \text{cm}^{-1}$ [8], $\mathcal{E}(5\,^3P_1) = 30\,665\ \text{cm}^{-1}$, $\mathcal{E}(6\,^3S_1) = 51\,498.4\ \text{cm}^{-1}$, and

$$\begin{aligned}\tilde{\nu}_{00}(E1 \leftarrow A0^+) &= \tilde{\nu}_{05} + G(v''=5) \\ &= 19\,774.5\ \text{cm}^{-1} + 159.1\ \text{cm}^{-1} \\ &= 19\,933\ \text{cm}^{-1}\ .\end{aligned} \tag{9}$$

$\mathcal{E}$ are energies of the atomic states and $\tilde{\nu}_{v'v''}$ are the wave numbers corresponding to $v' \leftarrow v''$ vibronic transitions. Equation (8) yields $D_0' = 1203.2\ \text{cm}^{-1}$ and we take the dissociation energy of the $E1$ state to be the average of the three closely lying values: $D_0'(E1) = 1200\ \text{cm}^{-1}$, with an estimated error of $\pm 0.3\%$ (the estimated errors on ω_0 and $\omega_0 x_0$ are 0.5%). This permits the identification of the lowest v' state in the v' progression since the transition corresponding to the longest-wavelength component in the spectrum must correspond to $v'=0$ in order that

$$\tilde{\nu}_{00} = \tilde{\nu}_{05} + G(v''=5) = 19\,933.6\ \text{cm}^{-1}\ .$$

This result leads to a value $D_0'(E1)$ equal to that obtained from the Birge-Sponer plot and based on the Morse approximation [19] and is also fully consistent with our conclusion reached from the spectroscopy of the $A0^+(5\,^3P_1)$

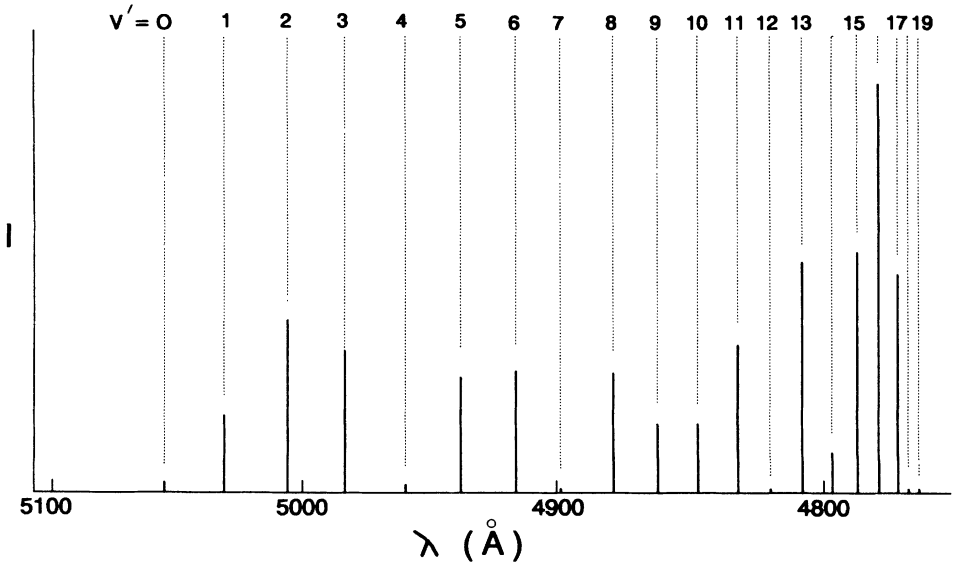

FIG. 6. Computer simulation of the $E1$, $v' \leftarrow A0^+$, $v''=5$ excitation spectrum, showing relative intensities of the vibrational components. The simulation indicates "missing" components corresponding to $v'=0$, 4, 7, and 12, which are also absent in Fig. 4(c).

TABLE II. Spectroscopic constants for CdAr.

Designation	$X0^+(5\,^1S_0)$[a]	$A0^+(5\,^3P_1)$[a]	$B1(5\,^3P_1)$[a]	$E1(6\,^3S_1)$[b]
ω_0 (cm^{-1})	18.9	38.1	11.1	102.8
$\omega_0 x_0$ (cm^{-1})	0.92	1.22	0.51	2.21
D_0 (cm^{-1})	97.0	303.0	54.0	1200.0
D_e (cm^{-1})	106.5	322	59.7	1252.8
ω_e (cm^{-1})	19.82	39.2	11.7	105.0
$\omega_e x_e$ (cm^{-1})	0.92	1.22	0.57	2.21
$r_e'-r_e''$ (Å)		-0.85 ± 0.01	0.70 ± 0.05	-0.61 ± 0.01
r_e(Å)	4.30 ± 0.04	3.45 ± 0.2	5.03 ± 0.03	2.84 ± 0.03

[a]Reference [8].
[b]This work.

state of CdAr that the assignment of the $v'=0$ state to the longest-wavelength component of a vibronic excitation spectrum leads to the correct D_0 value, a result that was also found in previous investigations [8].

The molecular constants obtained from a preliminary vibrational analysis of the spectrum were used, in conjunction with the Morse potential [19], to calculate the FC factors and produce a computer-simulated spectrum which is shown in Fig. 6 and whose intensity profile was fitted to that of the experimental spectrum, using $\Delta r_e = r_e' - r_e''$, the difference between the equilibrium internuclear separations of the $E1$ and $A0^+$ states, as an adjustable parameter to obtain the best fit. The molecular constants derived from this analysis are summarized in Table II. We found Δr_e to be very sensitive (±0.01 Å) to the fitting procedure and, since $r_e''=3.45$ Å has been determined previously [7,8], the analysis yielded $r_e'(E1)=2.84$ Å, a value consistent with the observed blue degradation of the vibrational components.

C. Identification of the "collisional" bands

The traces in Figs. 4(a) and 4(b) show a number of relatively broad components degraded to shorter wavelengths, which are not seen in Fig. 4(c). These collisional bands were produced as the result of inelastic collisions between the $A0^+(v''=5)$ molecules and Ar atoms, causing transfer to lower vibrational states. In the "warmer" part of the beam ($X/D=33$), some of the molecules could undergo up to two collisions per $A0^+$ lifetime. As may be seen in Table III, the pattern of the resulting additional vibrational components in the excitation spectrum is in full agreement with the separations $\Delta\tilde{\nu}$ that were accurately determined in the $A0^+(^3P_1)\leftarrow X0^+(^1S_0)$ spectrum of CdAr [8]. The quantities $\Delta G(v)$ in Table III give the energy differences between two adjacent $A0^+$ vibronic states and $\Delta\tilde{\nu}$ is the wave-number difference between the components arising from $v'=2\leftarrow v''=5$ and $v'=2\leftarrow v''=4$ transitions, etc. As the scan of the excitation spectrum reaches the energy corresponding to $v'=3$, the pattern of vibrational collisional components is repeated. For higher v' levels the wave-number separation of two consecutive collisional components decreases and the precise identification of the states and transitions becomes progressively more difficult. Figure 4(a) includes a sample assignment of two partial v'' progressions of collisional bands.

TABLE III. Collisional bands recorded in the $E1\leftarrow A0^+$ excitation spectrum [Fig. 4(a)] in the region of the $v'=2$–$v'=3$ components.

$v'\leftarrow v''$	$\tilde{\nu}$ (cm^{-1})	$\Delta\tilde{\nu}$ (cm^{-1})	$\Delta\tilde{\nu}$ (cm^{-1})[a]
2←5	19 982.0		
		26.5	27.0
2←4	19 955.5		
		28.7	28.8
2←3	19 926.8		
		30.0	31.0
2←2	19 896.8		

[a]Reference [8].

D. PE curves for the $X0^+$, $A0^+$, and $E1$ states of CdAr

The molecular constants listed in Table II were used, in conjunction with the Morse potential, to construct PE curves for the $X0^+$, $A0^+$, and $B1$ and $E1$ states, which are drawn in Fig. 7 together with theoretical curves calculated by Czuchaj and co-workers [14].

It may be seen that the theoretical and experimental [8] $X0^+$ curves show significant differences which are probably due to the fact that the theoretical curve was partly based on an incorrect value of D_e for the Cd_2 molecule [20], and the shape and location of the potential well (depth and r_e) were estimated with the aid of empirical mixing rules [21]. This gave rise to theoretical values $r_e=3.45$ Å and $D_e=264$ cm^{-1}, whereas our experimental values are 4.3Å and 106.5 cm^{-1}, respectively. On the other hand, there is very good agreement between the two curves for the $A0^+$ state with respect to both D_e and r_e, since the experimental values are 322 cm^{-1} and 3.45 Å, while the theoretical values are 328 cm^{-1} and 3.50 Å, respectively. We note that the theoretical curve for the $B1(^3P_1)$ state shows it to be repulsive while previous experiments [8] showed it to be weakly bound with $D_e=60$ cm^{-1}. Although we have no spectroscopic data that could be used to verify the $A0^-$ and $C2$ curves, a recent experiment of Bennett and Breckenridge [22] indicates that both these states in ZnAr are bound and have dissociation energies in excess of 300 cm^{-1}, suggesting that

TABLE IV. Estimated regions of bound-bound and bound-continuum fluorescence bands emitted from the $E1(^3S_1)$ state.

	Emission (Å)					
$E1 \leftarrow A0^+$	$E1(^3S_1) \rightarrow 2(^3P_2)$		$E1(^3S_1) \rightarrow A0^+(^3P_1)$		$E1(^3S_1) \rightarrow B1(^3P_1)$	
excitation	Bound-bound	Bound-cont.	Bound-bound	Bound-cont.	Bound-bound	Bound-cont.
$v'=2 \leftarrow v''=5$	5270-5360	> 5360	4970-5050	> 5050		
$v'=18 \leftarrow v''=5$	5020-5100	> 5100	4740-4815	> 4815		> 4820

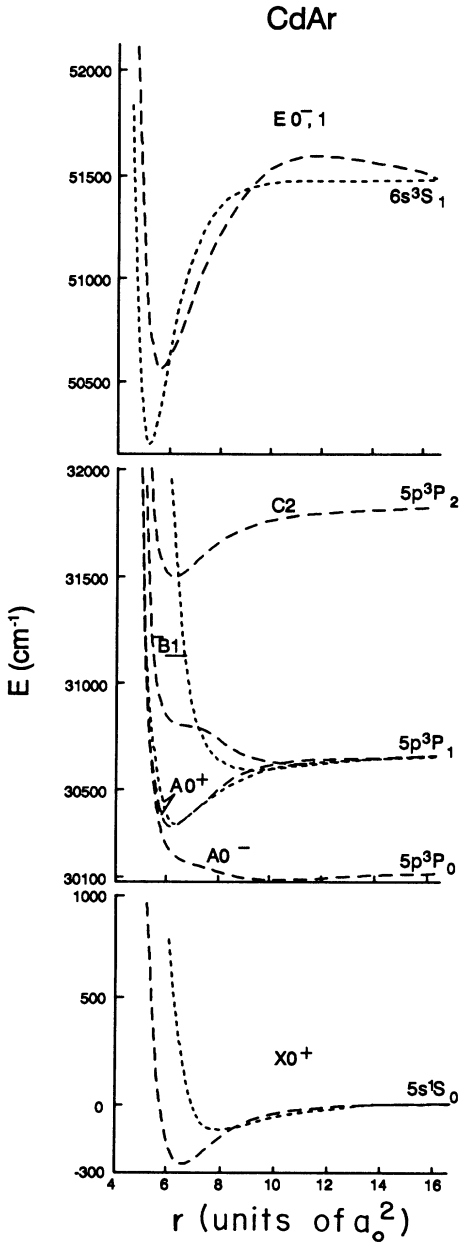

FIG. 7. A PE diagram for CdAr, showing curves calculated from experimental data using the Morse potential and curves derived from theoretical calculations [14]. The experimental curves for the $X0^+$, $A0^+$, and $B1$ states were taken from Ref. [8]. Short-dashed curve, experimental; long-dashed curve, theoretical.

they may also be bound in CdAr. Accordingly, the theoretical $D_e = 325\ \text{cm}^{-1}$ and $r_e = 3.3$ Å for the $C2(5\,^3P_2)$ state appear to be within the expected ranges, though the PE curve for the $A0^-(5\,^3P_0)$ state does not possess the anticipated bound character. Finally, there is reasonable agreement between the PE curves for the $E1$ state, though we found no indication of the potential barrier of about 120 cm^{-1}, predicted by the theory [14].

The PE curves derived from this experiment will be useful in predicting the spectral ranges of LIF spectra emitted from the $E1$ state. The LIF spectra that may be expected to be observed in a cold beam in the absence of collisions will depend on the wavelength of the exciting probe radiation. The spectral ranges of spectra excited from the $A0^+$, $v=5$ state, estimated on the basis of the FC principle, are indicated in Table IV. We have carried out some preliminary observations of LIF using wide-band filters, which tend to corroborate the information contained in Table IV.

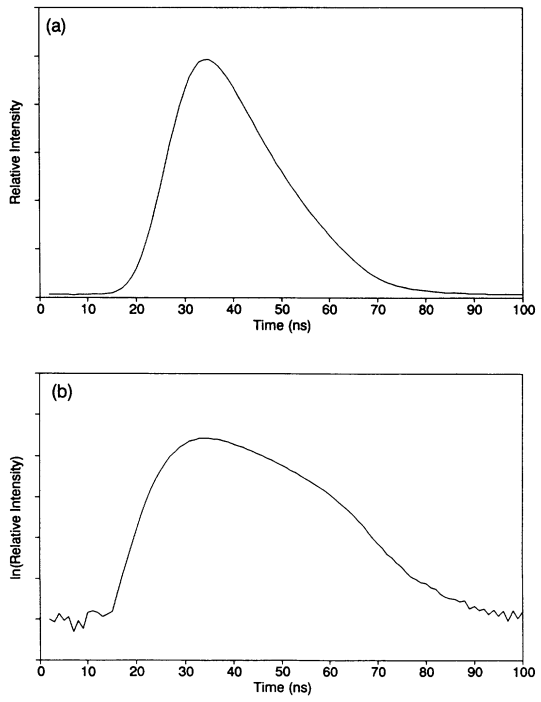

FIG. 8. Time evolution of CdAr fluorescence emitted from the $E1$, $v'=2$ state. (a) linear plot; (b) semilogarithmic plot.

E. The lifetime of the $E1$ state

In our recent studies of the $A0^+$ and $B1$ states of CdAr [8] we found that the lifetimes of the molecular vibronic states were generally shorter than the lifetime of the asymptotic atomic state. If the same situation applied in the case of the $E1$ state, then we might expect the $E1$ lifetime to be less than 15 ns, the lifetime of the $6\,^3S_1$ state [23]. The time evolution of the LIF emitted from the $E1$ state is shown in Fig. 8 which contains a linear and a semilogarithmic plot of LIF intensity against time, with 5005.9-Å probe laser radiation used for excitation ($v'=2\leftarrow v''=5$). It is evident that the decay is double exponential, and we believe that the component corresponding to the steeper slope and shorter lifetime represents the lifetime of the $E1$ state, while the longer-lived component is due to the "tail" of the scattered laser radiation. We estimate $\tau(E1)\cong 7$ ns, while the longer-lived component has a mean persistence time of about 13.5 ns. The relevant lifetimes are collected in Table V. We bear in mind that the time-evolution measurements were carried out on the total fluorescence output which essentially results from three transitions, $E1\rightarrow C2$, $A0^+$, $B1$, of which the latter makes a negligible or zero contribution to the fluorescence, an assumption based on the FC principle and inspection of Fig. 7. It is nevertheless evident that the $E1$ molecules decay very rapidly and, in a cold beam with $M_{\text{eff}}=62$, the time between collisions (estimated to be 10 μs) is very much longer than $\tau(E1)$ and consequently the $E1$ molecules in the beam may be regarded as moving in a collisionless environment. This result corroborates the previously reached conclusion that variations in the excitation spectrum arising from changes in the X/D parameter are due exclusively to collisions affecting the $A0^+$, v'' state.

TABLE V. Lifetimes τ (ns) of the atomic and molecular states.

CdAr $E1(6\,^3S_1)$	Cd $6\,^3S_1$
7.0[a]	17.0[b], 15.0[c]

[a]This work.
[b]Calculated from Ref. [14] (theoretical).
[c]Calculated from Ref. [23] (experimental).

[1] K. Fuke, S. Nonose, and K. Kaya, J. Chem. Phys. **85**, 1696 (1986).
[2] K. Yamanouchi, J. Fukuyama, H. Hiroguchi, S. Tsuchiya, K. Fuke, T. Saito, and K. Kaya, J. Chem. Phys. **85**, 1806 (1986).
[3] K. Yamanouchi, S. Isogai, M. Okunishi, and S. Tsuchiya, J. Chem. Phys. **88**, 205 (1988).
[4] T. Tsuchizawa, K. Yamanouchi, and S. Tsuchiya, J. Chem. Phys. **89**, 4646 (1988).
[5] A. Kowalski, M. Czajkowski, and W. H. Breckenridge, Chem. Phys. Lett. **121**, 217 (1985).
[6] A. Kvaran, D. J. Funk, A. Kowalski, and W. H. Breckenridge, J. Chem. Phys. **89**, 6069 (1988).
[7] D. J. Funk and W. H. Breckenridge, J. Chem. Phys. **90**, 2915 (1988).
[8] R. Bobkowski, M. Czajkowski, and L. Krause, Phys. Rev. A **41**, 243 (1990).
[9] M. Czajkowski, R. Bobkowski, and L. Krause, Phys. Rev. A **44**, 5730 (1991).
[10] I. V. Hertel, Adv. Chem. Phys. **45**, 341 (1981).
[11] M. Czajkowski, R. Bobkowski, and L. Krause, Phys. Rev. A **41**, 277 (1990).
[12] J. Wallace, R. R. Bennett, and W. H. Breckenridge, Chem. Phys. Lett. **153**, 127 (1988).
[13] M. Czajkowski, R. Bobkowski, and L. Krause, Phys. Rev. A **40**, 4338 (1989).
[14] E. Czuchaj and J. Sienkiewicz, J. Phys. B **17**, 225 (1984); E. Czuchaj, H. Stoll, and H. Preuss, *ibid.* **20**, 1487 (1986).
[15] C. T. Rettner and R. N. Zare, J. Chem. Phys. **77**, 2416 (1982).
[16] D. M. Lubman, C. T. Rettner, and R. N. Zare, J. Chem. Phys. **86**, 1129 (1982).
[17] R. M. Tennert, *Science Data Book* (Oliver and Boyd, Edinburgh, 1971).
[18] A. G. Gaydon, *Dissociation Energies* (Chapman and Hall, London, 1968).
[19] P. M. Morse, Phys. Rev. **34**, 57 (1929).
[20] H. Kuhn and S. Arrhenius, Z. Phys. **82**, 716 (1933).
[21] J. O. Hirschfelder, C. F. Curtiss, and R. B. Bird, *Molecular Theory of Gases and Liquids* (Wiley, New York, 1954).
[22] R. R. Bennett and W. H. Breckenridge, J. Chem. Phys. **92**, 1588 (1990).
[23] T. Andersen and W. Sorensen, J. Quant. Spectrosc. Radiat. Transfer **13**, 369 (1973).